robustness of the technique when dealing with real time series. A multiscale generalization, inspired by the multiscale entropy algorithm proposed by Costa et al. [24], is introduced for unveiling hidden information over different levels of temporal resolution of the original signal. The higher discriminative power at particular time scales observed in the physiological applications confirms the advantages of implementing the proposed multiscale analysis. As it will be shown below, our results demonstrate that the Abbe value and the number of turning points are two distinctive features for identifying differences in complex systems dynamics. Consequently, the location in the representation space, that results from computing simultaneously both quantifiers, deserves special consideration for time series classification purposes.

The remainder of this paper is structured as follows. In Section 2, the Tarnopolski's diagram together with the proposed multiscale recipe and a couple of benchmark tests are discussed. The performance of the method as a diagnostic tool is analyzed in Section 3 through several real-world applications. Finally, in Section 4, the main results and conclusions of this work are summarized.

2. Methods

2.1. Tarnopolski plane

Giving a time series $\{x_i\}_{i=1}^{n}$, the Abbe value, denoted $\mathcal{A}$ in this paper, is defined as half of the ratio of the mean square successive difference to the variance,

$$\mathcal{A} = \frac{n}{2(n-1)} \frac{\sum_{i=1}^{n-1}(x_{i+1}-x_i)^2}{\sum_{i=1}^{n}(x_i-\bar{x})^2} \tag{1}$$

with $\bar{x}$ the mean of $\{x_i\}$ [25–27]. The Abbe statistic quantifies the smoothness of a time series: it is close to zero for time series displaying a high degree of smoothness while it tends to one for white noise [23]. According to our knowledge, very few works have implemented this measure for practical applications. Within these few exceptions, the Abbe value and another related measure, the excess Abbe value, have been successfully applied in stellar variability studies for identifying transients in large-scale surveys [28].

A turning point in a time series is observed when the middle value x_i of a sequence of three consecutive observations is lower or higher than the other two values, x_{i-1} and x_{i+1}, that surround it [29]. Equal values, *i.e.* $x_j = x_k$ for $j \neq k$, are neglected. This assumption is justified whenever $\{x_i\}_{i=1}^{n}$ has a continuous distribution. From an arbitrary time series the probability of finding a turning point, denoted by $\mathcal{T}$, can be empirically estimated by its relative frequency. In particular, $\mathcal{T}$ is asymptotically equal to 2/3 for random time series. It is important to stress here that estimating the turning points probability is equivalent to calculate the zero crossing rate (ZCR) of the differentiated time series. ZCR has been previously implemented for diverse applications, *e.g.* the detection of voiced and unvoiced sounds in speech signals [9] and the automatic diagnosis of tonic-clonic epileptic seizures [30]. The probability of finding a turning point is also linked with ordinal patterns. Indeed, estimating $\mathcal{T}$ is equivalent to calculate the relative frequency of four of the six possible motifs when embedding dimension $D = 3$ is considered (please see permutation indices 2, 3, 4 and 5 in Fig. 2a of Ref. [21]).

Tarnopolski introduced a model representation space by plotting the fraction of turning points of a time series versus its associated Abbe value. This $\mathcal{T}$ vs $\mathcal{A}$ diagram is able to discriminate fBm, fGn and dfGn (please see Fig. 5 of Ref. [23]). Moreover, an invertible relationship is found between $\mathcal{A}$ and the Hurst exponent H. This functional form has been then used for estimating the Hurst exponent of several real world data. Briefly, the Hurst exponent H is a scaling exponent that measures the long-range dependence in time series. Further details about H can be found in Refs. [31,32]. For illustrating the ability of the Tarnopolski plane to characterize long-range dependence in time series, we have analyzed the location of generic $1/f^{\alpha}$ noises in this bidimensional scheme. In Fig. 1 a), we depict the position of colored noises with α ranging from -1 to 3 in steps of size 0.1. Average and standard deviation (SD) (displayed as error bars) of estimated $\mathcal{A}$ and $\mathcal{T}$ values for one hundred independent realizations of length $n = 2^{14}$ for each α exponent have been plotted. The Fourier Filtering Method (FFM) has been implemented in Matlab for generating these long-range power-law correlated time series. In the FFM, the Fourier components of an uncorrelated sequence of Gaussian-distributed random numbers are filtered with a suitable power-law filter in order to introduce correlations among the variables. We address the reader to Refs. [33,34] for more details about this algorithm. Some examples of these artificial long-range correlated time series are shown in Fig. 1 b). It can be concluded that colored noises with α between -1 and 1 are more noisy and better discriminated by the Abbe value. Whereas, when the power-law exponent is between 1 and 3, the fraction of turning points is more appropriate for distinguishing between them. We have also confirmed that a very similar evolution in the Tarnopolski plane is followed by longer $1/f^{\alpha}$ artificial time series ($n = 100{,}000$). As expected, in this case, shorter SD error bars are obtained.

2.2. Multiscale analysis

It is widely recognized that time series arising from some representative variable of nonlinear complex systems have a multiscale nature, *i.e.* the observed dynamics is often strongly dependent on the resolution scale used to sample the signal. For illustrating this multiscale phenomenon, we consider the analysis of time series derived from nonlinear dynamics in a numerically controlled situation. More precisely, we estimate $\mathcal{A}$ and $\mathcal{T}$ from realizations of the x-variable of the Lorenz system:

$$\dot{x} = \sigma(y-x), \quad \dot{y} = x(\rho - z) - y, \quad \dot{z} = xy - \beta z\,. \tag{2}$$

Following the example included in Ref. [23], time series of length $n = 2^{14}$ data points were generated with initial conditions $(x_0, y_0, z_0) = (1, 5, 10)$, and standard parameters $\sigma = 10$, $\rho = 28$ and $\beta = 8/3$ for which the system exhibits chaotic behavior. The time series were numerically integrated by using the Matlab's *ode45* function, that implements fourth and fifth order Runge–Kutta numerical integration algorithms, with an integration step equal to 0.001. Sampling periods δ_t ranging from 0.001 to 1 with a step equal to 0.001 are considered. We analyzed time series with $n = 2^{14}$ data points for each δ_t. The first 10^5 iterations were discarded to avoid possible transients. The evolution of the location in the Tarnopolski plane of these one thousand numerical realizations of length $n = 2^{14}$ with different temporal resolutions is depicted in Fig. 2. It is worth remarking here that a very similar behavior is obtained by analyzing longer numerical realizations ($n = 100{,}000$). On the one hand, for low values of δ_t, an artificial regular behavior is spuriously observed due to oversampling and both quantifiers are near zero. This oversampling generates redundancy in the information contained in the signals. On the other hand, for high values of the sampling period, the signal appears to be stochastic and fully uncorrelated. Essentially, relevant information about the nonlinear temporal correlations is lost due to undersampling, and the value of quantifiers are close to that expected for a white noise, *i.e.* $\mathcal{A} \approx 1$ and $\mathcal{T} \approx 2/3$. Through this toy example it is easily concluded that the estimated value for $\mathcal{A}$ and $\mathcal{T}$, and consequently the location in the bidimensional scheme, is strongly dependent on the temporal resolution. These findings imply the need to explicitly include the time scale notion in the implemented measure to reach a more proper characterization.

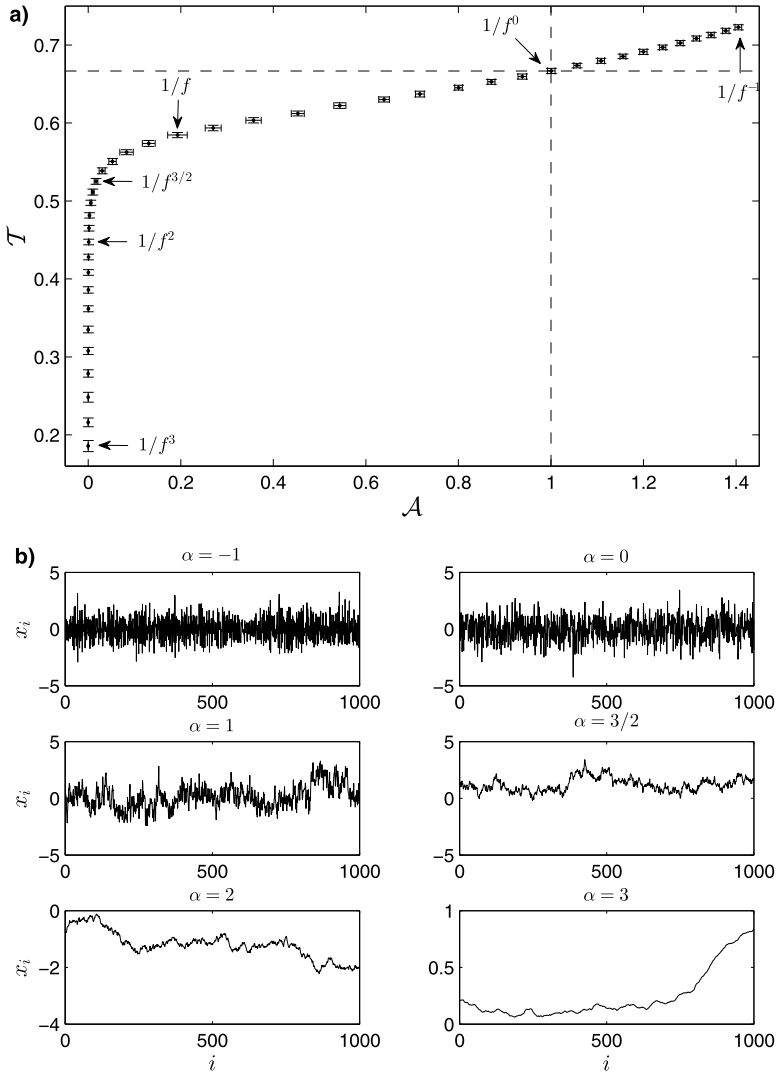

Fig. 1. a) Location in the Tarnopolski representation space of generic $1/f^{\alpha}$ noises with $\alpha \in \{-1, -0.9, ..., 3\}$. One hundred numerical realizations of length $n = 2^{14}$ data points for each α exponent were generated with FFM. Mean and standard deviation (displayed as error bars) of estimated values for both quantifiers, $\mathcal{A}$ and $\mathcal{T}$, over these one hundred simulations are shown. Positions of quantifiers move gradually from the right upper corner to the left bottom corner as α increases. Horizontal and vertical dashed lines indicate the theoretical value of quantifiers for white noise stochastic processes. b) Some examples of the numerically generated long-range power-law linearly correlated time series. Only 10^3 data points are plotted for a better visualization.

Multiscale entropy [24] and scale-dependent Lyapunov exponents [35] are two generalized quantifiers introduced precisely with the aim of characterizing the different signal behaviors on a wide range of scales simultaneously. Bearing in mind the inherent scale-dependent nature of the physiological systems we will analyze in the next section, a multiscale tool is proposed by constructing coarse-grained time series at multiple temporal scales and estimating the statistical quantifiers $\mathcal{A}$ and $\mathcal{T}$ for each of these transformed time series. Coarse-grained sequences are reconstructed by following the same procedure introduced in Ref. [24]. That is, the original record of length n is divided into non-overlapping segments of length τ, and the mean value is calculated for each segment generating smoothing sequences $\{y_j^{\tau}\}$ of length $\lfloor n/\tau \rfloor$,

$$y_j^{\tau} = \frac{1}{\tau} \sum_{i=(j-1)\tau+1}^{j\tau} x_i, \quad 1 \leq j \leq \lfloor n/\tau \rfloor \tag{3}$$

with $\lfloor n/\tau \rfloor$ the largest integer not greater than n/τ. The analysis of the location of both quantifiers, $\mathcal{A}$ and $\mathcal{T}$, in the Tarnopolski plane as a function of the temporal scale factor τ allows detection of intrinsic complex structures across multiple temporal resolutions. Furthermore, the identification of optimal time scales for the classification of complex systems could be achieved by implementing this approach. For checking the usefulness of this multiscale recipe, we have analyzed an oversampled long numerical realization of the x-variable of the Lorenz system with the same parameters and initial conditions detailed previously. The chosen sampling period was $\delta_t = 0.001$ and the time series length $n = 2^{24}$. A multiscale analysis with temporal scale factors $1 \leq \tau \leq 1000$ has been performed. Evolution of the location of quantifiers for these temporal scales is depicted in Fig. 3 (blue curve). The evolution obtained for the original analysis for different sampling period developed previously is also plotted (black curve) for the sake of comparison. Overall, the results are qualitatively similar. The observed quantitative differences are attributed to the non-overlapping moving average filter (Eq. (3)) proposed for constructing the coarse-grained time series.

3. Real-world applications

Time series generated in a wide range of fields ranging from physiology to economy result from very complex dynamics and/or from coupled dynamics of many dimensional systems. Besides,

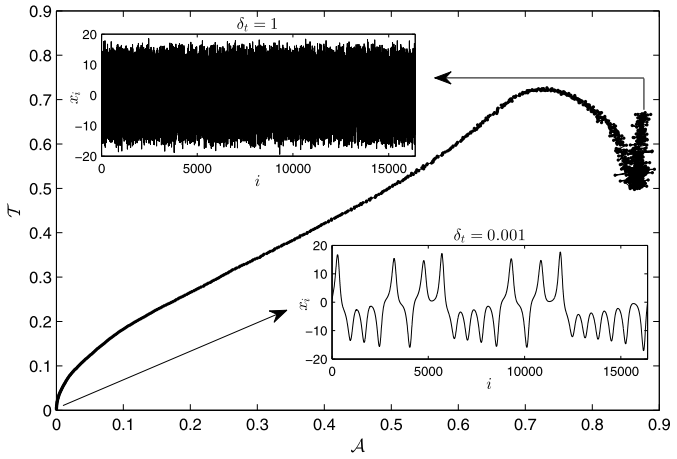

Fig. 2. Location in the Tarnopolski plane of one thousand numerical realizations of the x-variable of the Lorenz system ($\sigma = 10$, $\rho = 28$, $\beta = 8/3$, and $(x_0, y_0, z_0) = (1, 5, 10)$) with different sampling periods ($\delta_t \in \{0.001, 0.002, ..., 1\}$). Time series of length $n = 2^{14}$ data points were generated with initial conditions $(x_0, y_0, z_0) = (1, 5, 10)$. Positions of quantifiers move gradually from the left bottom corner to the right upper corner as δ_t increases. Simulations of the x-variable for the two extreme sampling periods, *i.e.* $\delta_t = 0.001$ and $\delta_t = 1$, are shown in the lower and upper insets, respectively. A similar evolution has been confirmed for longer numerical realizations ($n = 100{,}000$).

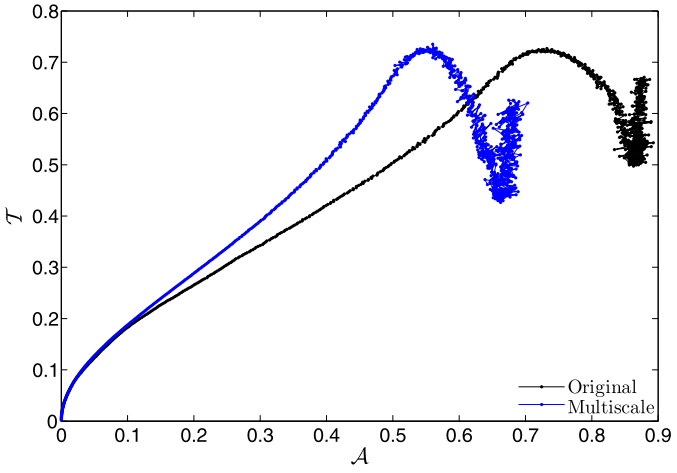

Fig. 3. Evolution of location in the Tarnopolski plane for an oversampled ($\delta_t = 0.001$) and long ($n = 2^{24}$) numerical realization of the x-variable of the Lorenz system ($\sigma = 10$, $\rho = 28$, $\beta = 8/3$, and $(x_0, y_0, z_0) = (1, 5, 10)$) by implementing a multiscale analysis with temporal scale factor τ ranging from 1 to 1000 (blue curve). Positions of quantifiers move gradually from the left bottom corner to the right upper corner as τ increases. The original evolution obtained for different sampling periods is also displayed (black curve) for easy comparison. (For interpretation of the references to color in this figure legend, the reader is referred to the web version of this article.)

these real signals are often contaminated by noise and other artifacts. Thus, the extraction of meaningful information from them is usually a challenging task. Taking this into account, next we will test the efficiency of the Tarnopolski representation space in real situations.

3.1. Efficiency of developed, emerging and frontier stock markets

It is well-known that a stock market is considered efficient whenever its prices follow a random walk. That is, the increments of the prices should be independent and obey a Gaussian distribution. However, it is also widely accepted that this is only an idealized first approximation, and deviations from this white noise model, violating either the independence or Gaussian assumptions, have been found in many empirical studies since the revolutionary paper of Benoit Mandelbrot [36]. In particular, correlated markets open the door to arbitrage opportunities because past prices can help to predict future prices. Indeed, it has been shown that emerging markets have greater correlations than developed ones, suggesting more predictability [37,38]. Moreover, the Hurst exponent has been widely proposed to quantify the stock market efficiency [39–43].

Given the link found between the Hurst exponent and the two statistical quantifiers that define the Tarnopolski plane, we propose to use this representation space to distinguish the stage of stock market development. With this aim in mind, we analyze the price returns of forty-eight stock market indices for different countries. Codes and names of these indices, collected from the Datastream platform (http://financial.thomsonreuters.com/en/products/tools-applications/trading-investment-tools/datastream-macroeconomic-analysis.html), are detailed in Table 1. Daily prices beginning on January 3, 2000 and ending on May 27, 2016 are considered (4,280 observations). Following the classification provided by the Morgan Stanley Capital Index (MSCI) methodology (https://www.msci.com), there are twenty developed, seventeen emerging and eleven frontier stock markets.

Locations in the $\mathcal{T}$ vs $\mathcal{A}$ diagram of the daily price returns of the forty-eight stock market indices are plotted in Fig. 4. Mean and standard deviation (displayed as error bars) of one thousand numerical independent realizations of fGn with Hurst exponents $H \in \{0.05, 0.10, ..., 0.95\}$ and the same length of the returns ($n = 4{,}279$) are also shown. These simulations were obtained by consecutive differences of fBm generated via the MATLAB function *wfbm*. On the one hand, it is observed that positions of indices associated with developed countries (blue circles) are, in average, closer to the ideal efficiency point, *i.e.* $\mathcal{A} \approx 1$ and $\mathcal{T} \approx 2/3$, that corresponds to white noise. Particularly, price returns of the American stock market index (Standard & Poor's 500) show an antipersistent behavior and, according to its location in the Tarnopolski plane, could be modeled as a fGn with $H = 0.45$. On the other hand, price return indices of stock market from emerging countries (green triangles) have lower estimated values for both quantifiers confirming the presence of persistency in their dynamics. There are two exceptions, namely Thailand ($\mathcal{A} \approx 0.987$, $\mathcal{T} \approx 0.661$) and Turkey ($\mathcal{A} \approx 1.006$, $\mathcal{T} \approx 0.662$), located within the region of maximum efficiency. Finally, price return indices of frontier countries (red squares) can be considered as the most inefficient since they are more distant with respect to the white noise location. The presence of strong long-range correlations in their dynamics is the main reason of this inefficient location. Argentina ($\mathcal{A} \approx 0.945$, $\mathcal{T} \approx 0.649$) and Croatia ($\mathcal{A} \approx 0.911$, $\mathcal{T} \approx 0.653$) are the two frontier countries whose price return indices appear to be better behaved (please see the two red squares nearest to the ideal efficiency location). It is also worth noting that the positions of all indices are below the curve described by the family of fGn. We conjecture that this behavior could be attributed to non-Gaussian distributions. It is then concluded that the fGn stochastic processes do not seem to be suitable for modeling the price returns of stock market indices of many emerging and frontier countries. This is especially clear in the case of Oman index ($\mathcal{A} \approx 0.819$, $\mathcal{T} \approx 0.555$). We confirm, through this financial application, that the Tarnopolski bidimensional scheme is a powerful tool for discriminating market dynamics since it is able to distinguish simultaneously different degrees of correlations and deviations from Gaussianity. The daily original resolution, that is $\tau = 1$, has been used in this analysis since improvements in the classification are not observed for larger temporal scales $2 \leq \tau \leq 10$. Indeed, for the larger scale factors ($\tau \geq 5$), locations of the different countries overlap in a small region making the distinction between the three groups almost impossible. Qualitatively similar findings have been confirmed for the same database but in a shorter data span (since January 1, 2010 to

Table 1
Codes and names of the stock market indices downloaded from Datastream. Developed, emerging and frontier stock markets (classified following the MSCI methodology) are denoted as D, E and F, respectively.

Country	Datastream code	Index	MSCI classification
1. Netherlands	AMSTEOE	AEX INDEX (AEX)	D
2. Jordan	AMMANFM	AMMAN SE FINANCIAL MARKET	F
3. Argentina	ARGMERV	ARGENTINA MERVAL	F
4. Greece	GRAGENL	ATHEX COMPOSITE	E
5. Austria	ATXINDX	ATX – AUSTRIAN TRADED INDEX	D
6. Thailand	BNGKSET	BANGKOK S.E.T.	E
7. Belgium	BGBEL20	BEL 20	D
8. Turkey	TRKISTB	BIST NATIONAL 100	E
9. Hungary	BUXINDX	BUDAPEST (BUX)	E
10. Chile	IGPAGEN	CHILE SANTIAGO SE GENERAL (IGPA)	E
11. Sri Lanka	SRALLSH	COLOMBO SE ALL SHARE	F
12. Croatia	CTCROBE	CROATIA CROBEX	F
13. Germany	DAXINDX	DAX 30 PERFORMANCE	D
14. Egypt	EGHFINC	EGYPT HERMES FINANCIAL	E
15. France	FRCAC40	FRANCE CAC 40	D
16. United Kingdom	FTSE100	FTSE 100	D
17. Malaysia	FBMKLCI	FTSE BURSA MALAYSIA KLCI	E
18. Italy	FTSEMIB	FTSE MIB INDEX	D
19. South Africa	JSEOVER	FTSE/JSE ALL SHARE	E
20. Hong Kong	HNGKNGI	HANG SENG	D
21. Hong Kong	HKHCHAF	HANG SENG CHINA AFFILIATED CORP	D
22. Hong Kong	HKHCHIE	HANG SENG CHINA ENTERPRISES	D
23. Spain	IBEX35I	IBEX 35	D
24. Indonesia	JAKCOMP	IDX COMPOSITE	E
25. Ireland	ISEQUIT	IRELAND SE OVERALL (ISEQ)	D
26. Israel	ISTA100	ISRAEL TA 100	D
27. Pakistan	PKSE100	KARACHI SE 100	F
28. Kenya	NSEINDX	KENYA NAIROBI SE (NSE20)	F
29. Korea	KORCOMP	KOREA SE COMPOSITE (KOSPI)	E
30. Lebanon	LBBLOMI	LEBANON BLOM	F
31. Germany	MDAXIDX	MDAX FRANKFURT	D
32. Mexico	MXIPC35	MEXICO IPC (BOLSA)	E
33. Oman	OMANMSM	AN MUSCAT SECURITIES MKT.	F
34. Denmark	COSEASH	OMX COPENHAGEN (OMXC)	D
35. Finland	HEXINDX	OMX HELSINKI (OMXH)	D
36. Sweden	SWSEALI	OMX STOCKHOLM (OMXS)	D
37. Estonia	ESTALSE	OMX TALLINN (OMXT)	F
38. Philippine	PSECOMP	PHILIPPINE SE I(PSEi)	E
39. Czech Republic	CZPXIDX	PRAGUE SE PX	E
40. Romania	RMBETRL	ROMANIA BET (L)	F
41. Russia	RSMICEX	RUSSIAN MICEX INDEX	E
42. USA	S&PCOMP	S&P 500 COMPOSITE	D
43. China	CHSASHR	SHANGHAI SE A SHARE	E
44. China	CHZBSHR	SHENZHEN SE B SHARE	E
45. Switzerland	SWISSMI	SWISS MARKET (SMI)	D
46. Taiwan	TAIWGHT	TAIWAN SE WEIGHED TAIEX	E
47. Japan	TOKYOSE	TOPIX	D
48. Tunisia	TUTUNIN	TUNISIA TUNINDEX	F

May 27, 2016). Comparison of the performance of the Tarnopolski representation space with other implemented tools for characterizing financial data efficiency, such as entropy-related methodologies [44–47] and the Efficiency Index [48–50], is beyond the purpose of the present work and will be studied in a future research.

3.2. *Electroencephalograms from healthy and epileptic patients*

Discrimination of brain electrical activity from different regions and from different physiological and pathological brain states is obviously a very relevant issue since this information could be potentially useful for medical diagnosis. Motivated by this fact, we analyze five different sets of electroencephalogram (EEG) time series for different groups and recording regions: surface (scalp) EEG recordings from five healthy volunteers in an awake state with eyes open (Set A) and closed (Set B), intracranial EEG recordings from five epilepsy patients during the seizure free interval from outside (Set C) and from within (Set D) the seizure generating area, and intracranial EEG recordings of epileptic seizures (Set E). These artifact-free records are available under www.meb.unibonn.de/epileptologie/science/physik/eegdata.html. The sampling rate of the data was 173.61 Hz. One hundred single channel EEG segments of 23.6 s of duration (4,097 data points) for each one of the five sets of data have been considered. These segments were selected from continuous multichannel EEG recordings after visual inspection for artifacts (*e.g.* muscle activity or eye movements). Additionally, only segments that satisfy a weak stationarity criterion were chosen. Further details about the recording technique of these EEG data can be found in the original paper by Andrzejak et al. [51].

Taking into account that the optimal time scale for discriminating these five sets of EEG data is *a priori* not known, a multiscale analysis has been implemented. That is, we have analyzed the location in the Tarnopolski diagram for coarse-grained time series with temporal scale factors $1 \leq \tau \leq 10$. Mean and standard deviation (displayed as error bars) of the one hundred $\mathcal{A}$ and $\mathcal{T}$ values computed for the five EEG sets have been plotted for the different resolution temporal scales. Fig. 5 shows the results obtained for four different temporal scales ($\tau \in \{1, 4, 7, 10\}$). It is visually

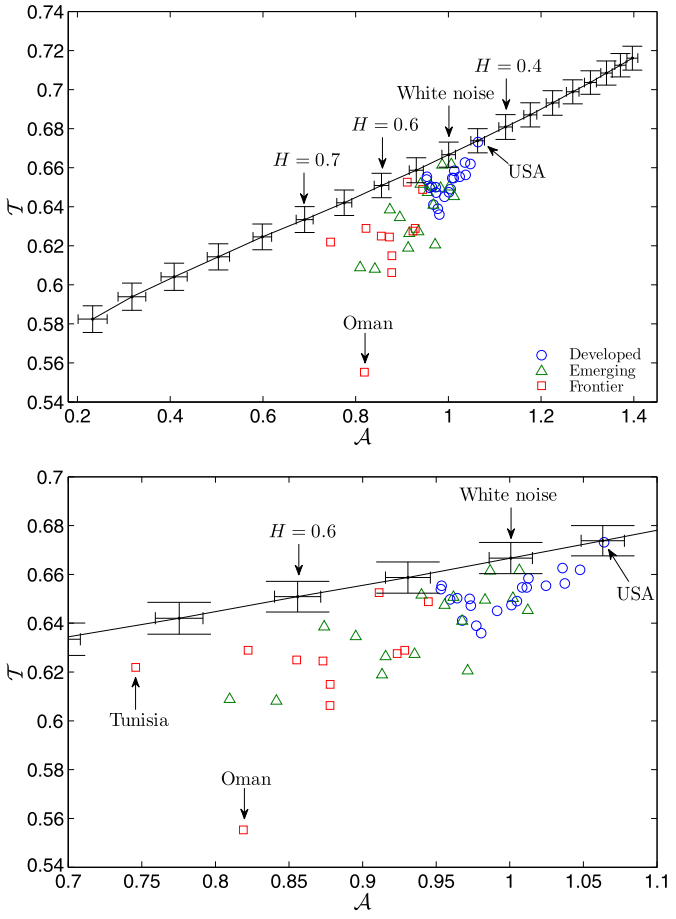

Fig. 4. Top: Position of the price returns of the forty-eight stock market indices in the Tarnopolski plane. Developed, emerging and frontier countries are identified by blue circles, green triangles and red squares, respectively. Location of fGn with Hurst exponents $H \in \{0.05, 0.10, ..., 0.95\}$ and the same length of the price returns ($n = 4{,}279$) has been also included. Being more precise, mean and standard deviation (displayed as error bars) of one thousand independent realizations are depicted in black color. A continuous black curve joining the mean values for fGn with different H is included for visual reference. Estimated values for both quantifiers decrease as the Hurst exponent of fGn increases. Bottom: Enlargement for a better view of locations associated with stock market indices. (For interpretation of the references to color in this figure legend, the reader is referred to the web version of this article.)

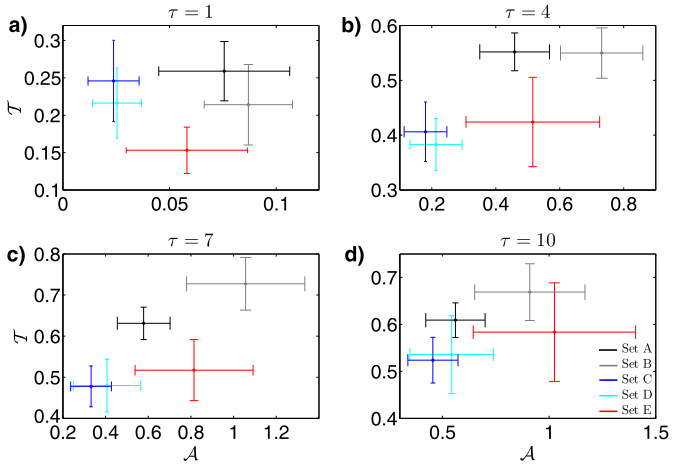

Fig. 5. Location of the five sets of EEG data in the Tarnopolski plane for different temporal scale factors: a) $\tau = 1$, b) $\tau = 4$, c) $\tau = 7$, and d) $\tau = 10$. Mean and standard deviation (displayed as error bars) of both quantifiers, $\mathcal{A}$ and $\mathcal{T}$, for the one hundred single channel EEG segments associated with each set are plotted. Groups are differentiated by color: Set A in black, Set B in gray, Set C in blue, Set D in cyan, and Set E in red. (For interpretation of the references to color in this figure legend, the reader is referred to the web version of this article.)

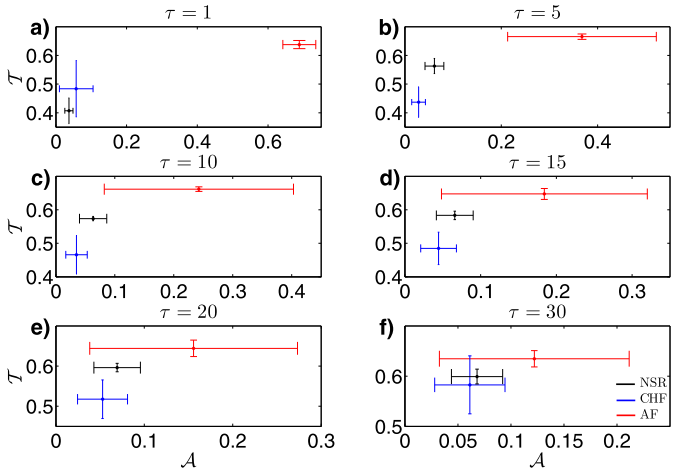

Fig. 6. Location of the three groups of HRV data in the Tarnopolski plane for different temporal scale factors: a) $\tau = 1$, b) $\tau = 5$, c) $\tau = 10$, d) $\tau = 15$, e) $\tau = 20$, and f) $\tau = 30$. Mean and standard deviation (displayed as error bars) of both quantifiers, $\mathcal{A}$ and $\mathcal{T}$, for the five BBI time series associated with each set are plotted. Groups are differentiated by color: NSR in black, CHF in blue, and AF in red. (For interpretation of the references to color in this figure legend, the reader is referred to the web version of this article.)

confirmed that an improved classification is reached for intermediate resolution scales. In such a case not only healthy (Sets A and B) and pathological groups (Sets C, D and E) are discriminated, but also differences between interictal (Sets C and D) and ictal activities (Set E) are achieved. Regrettably, interictal epileptiform activities from the epileptogenic zone (Set D) and those found at recording sites distant from the epileptogenic zone (Set C) cannot be separated. Last but not least, for these intermediate temporal scales, the two healthy groups are clearly distinguished. This differentiation between the conditions of eyes closed and eyes open has not been reached by previous implemented algorithms much more complicated, both computationally and conceptually [18,51–53]. We consider this a very interesting finding since it is well-known that alpha waves in a frequency range of 8–13 Hz are predominant in relaxed healthy subjects with eyes closed while broader frequency characteristics are obtained for open eyes [51].

3.3. *Physiological and pathological beat-to-beat intervals*

In this application, heart rate variability (HRV) of healthy and pathological subjects have been analyzed. HRV time series are derived from electrocardiogram signals by measuring consecutive beat-to-beat intervals (BBI). As cardiac diseases have effects on BBI dynamics, a reliable classification between physiological and pathological BBI time series could be useful for developing a new diagnostic tool [21]. Three different groups have been considered in our analysis. More precisely, the location in the Tarnopolski representation space for a total of fifteen BBI time series of which five were obtained from healthy persons in normal sinus rhythm (NSR), five from congestive heart failure (CHF) patients, and five from subjects suffering from atrial fibrillation (AF), have been tested. These records, freely available in PhysioNet (www.physionet.org/challenge/chaos/), are about 24 h long (roughly 100,000 intervals). Filtered records, *i.e.* with outliers removed, were used. We have again implemented a multiscale analysis by estimating both quantifiers, $\mathcal{A}$ and $\mathcal{T}$, for coarse-grained time series with $1 \leq \tau \leq 30$. In Fig. 6, we have plotted mean and standard deviation (displayed as error bars) of these quantifiers for the three HRV groups (NSR, CHF and AF)